On the near-wall structure in reverse-flow and post-reattachment recovery regions of separated flow and its equivalence to the structure in wall and free-surface jets

A. Dejoan and M.A. Leschziner
Department of Aeronautics, Imperial College London,
London SW7 1AZ, UK.
Email: a.dejoan@imperial.ac.uk, mike.leschziner@imperial.ac.uk

Abstract

The statistical and structural properties of two wall jets, one developing along a real wall and the other along a shear-free wall, are contrasted with the equivalent properties in the post-reattachment-recovery and reverse-flow regions of a separated backward-facing step flow, respectively. The study was motivated, principally, by the wish to isolate and understand the mechanisms responsible for the poor representation of the post-reattachment recovery returned by most RANS closures. It demonstrates a substantive commonality in the turbulent processes between, on the one hand, the real wall jet and post-reattachment recovery, and on the other hand, between the zero-wall-shear jet and the reattachment zone, as well as the reverse-flowing near-wall layer in the backward-facing-step flow. All regions under consideration are found to be characterised by an influential interaction between an outer shear layer and the wall, but an important distinction arises from the presence or absence of strong near-wall shear, which introduces significant changes to the nature of this interaction: in the absence or near-absence of wall shear, the interaction is largely inviscid, associated with wall-blocking, while strong shear tends to shield the wall from the outer flow. The commonality between the two sets of flow conditions is explored by way of mean-flow properties, budgets, anisotropy maps, departures from local equilibrium, non-dimensional strain parameter, length-scale variations and structural properties. The study shows that the post-reattachment-recovery region, like the real wall jet, is far from the state local equilibrium found in a standard boundary layer, that the recovery of the flow towards a state equilibrium is slow, and that the near-wall region is strongly affected by turbulent diffusion associated with the migration of large-scale structures towards the wall. In statistical terms, this last process is represented by the importance of turbulent transport by third moments and pressure-velocity correlations. Within the reattachment and reverse-flow layer, near-wall shear is weak, and so is the shielding of the wall from the outer layer. In these regions, the flow shares many of the properties of the zero-wall-shear jet.

Keywords: Large eddy simulation, wall jets, backward-facing step flow, turbulence budgets, turbulence structure, separation, reattachment, post-reattachment recovery

1 Introduction

The correct prediction of separation over a broad range of geometric and flow conditions remains a major challenge to even the most advanced turbulence models, at whatever level of closure [1], [2]. Although the overall features and dimensions of separated zones are returned correctly by some turbulence models, the velocity and Reynolds-stress fields are almost always poorly predicted. One particular defect, observed irrespective of the quality of model solutions within the recirculation zone itself, is an insufficient rate of post-reattachment recovery. The ubiquity of this defect suggests that the problem may lie in the complex interaction between the outer shear layer, originally above the recirculation zone, and the wall over which the wake recovers. Fig. 1 gives a schematic view of the major interactions of interest herein and described below. The effect of the wall is two-fold: first, it acts to block the wall-normal velocity fluctuations and to reflect pressure fluctuations, thus modifying the turbulence field away from the wall in the shear layer; and second, it causes the formation of a sheared boundary layer, with its own scales and turbulence characteristics, which interacts with the outer shear layer, thus affecting its evolution. Within the recirculation zone itself, the near-wall backward flow may also be regarded as an amalgam of (at least) two disparate shear layers: the outer one originating from the lower part of the post-separation free shear layer, subjected to strong curvature as a consequence of reattachment, and the inner one being the boundary layer originating at the reattachment point line. However, here, the boundary layer is very thin, and the flow is, most likely, dominated by the outer shear layer interacting almost inviscidly with the wall. Both the post-reattachment recovery layer and the reverse-flow layer are highly perturbed, in addition to being composite layers, by the strong curvature and normal straining associated with the impingement process in the reattachment region.

It is the above two-pronged interaction between composite shear layers and the wall that is the focus of the present study. Its principal objective is to gain insight into the peculiar characteristics of the turbulence processes within the shear layers in the wake recovering from separation and reattachment and in the near-wall layer within the recirculation zone. A second objective is to derive from this insight the implications for modelling recirculating flows, with the emphasis being placed on the recovery zone.

In this context, a flow that appears to be highly pertinent to post-reattachment recovery is the wall jet. This flow also consists of two interacting shear layers, one a separated outer layer and the other a boundary layer. The turbulence processes in this flow have recently been the subject of three studies by the present authors [3], [7], [4], in which data derived from large eddy simulations have been analysed. These studies focus, respectively, on the turbulence structure of the wall jet, on the discrimination of effects arising from wall blocking and wall shear and on a-priori studies of elements of second-moment RANS closures. Some important features that the simulations have brought out include the significant contribution of triple-correlations-driven stress diffusion in the interaction region, the surprisingly high level of pressure diffusion, the strong influence of wall blocking on the redistribution mechanism and the major effects on the turbulence structure brought about by the addition of near-wall shear to wall blocking. An outcome of the a-priori RANS studies [4] has been the illumination of some of the reasons for the poor representation of the above-noted features by popular second-moment-closure models.

The present study contrasts the turbulence characteristics of the recovery and reverse-flow layers of the separated flow behind a backward-facing step against those of two wall jets, one with and the other without wall shear, the comparative analysis being based, principally, on Reynolds-stress budgets and observations of structural properties. The back-step-flow simulations were undertaken by the present authors in the context of a study on the control of separation by means of a synthetic jet [5], which perturbs the

separated shear layer. Here, the data for the unperturbed flow are exploited. The rationale is to identify parallels in the turbulence mechanisms and to understand the extent to which the supposition of the equivalence of the processes in the regions of interest within the recirculating flow and the jets is valid. As will emerge, there are indeed a number of fundamental statistical mechanisms that link the two flows, despite the self-evident differences in their global characteristics.

2 The flow configurations and their simulations

The flow configurations studied are shown in Fig. 2, and the numerical parameters of the simulations are summarised in Table 1. The back-step flow is at a Reynolds number $Re = U_c h/\nu = 3700$, at conditions identical to those of the experiments of Yoshioka *et al.* [6]. The computational domain extends from $4h$ upstream of the step to $18h$ downstream. The spanwise direction is statistically homogeneous and $4\pi/3$ deep. A two-block grid of 2.10^6 nodes is used, with the maximum ratio of the grid scale, Δ, to the Kolmogorov scale, η, not exceeding 7 throughout the domain, see top Fig. 3. The maximum value of $y^+ = yu_\tau/\nu$ at both the lower and upper walls is less than 1, and the cell-aspect ratio is, typically, $\Delta y^+/\Delta x^+/\Delta z^+ = 1.1/18/10$ at the wall and 2.5/18/10 in the shear layer. The inlet conditions, prescribed at $4h$ upstream the step, were derived from a fully-developed channel-flow precursor computation carried out over a domain of $2h \times 2\pi h \times 4\pi h$ with streamwise-periodicity imposed.

The wall jet is at a Reynolds number $Re = U_o b/\nu = 9600$, U_o being the inlet velocity and b the slot height. Two cases were simulated, one in which the jet develops along a real wall and the other along a frictionless, impermeable boundary. Here, the intention is to permit effects arising from wall-blocking and near-wall shear to be distinguished or separated within the whole interaction process between the outer shear layer and the wall. The real jet simulated corresponds to one studied experimentally by Eriksson *et al.* [9]. In both jet flows, the domain extends from the wall to $10b$ above it and to $22b$ in the streamwise direction. The grid is composed of 8.10^6 computational cells, and the ratio Δ/η is typically $5 - 10$, see middle and bottom plots of Fig. 3. For the real jet, the near-wall cell-aspect ratio is, typically, $\Delta y^+/\Delta x^+/\Delta z^+ = 1.2/24/24$, the wall-nearest grid node located at $y^+ = 0.6$. More details can be found in [3], [7].

Computational tests, including the use of different grid-resolution levels and subgrid-scale models, have shown the back-step-flow simulation to be insensitive to subgrid-scale modelling, and the standard (wall-damped) Smagorinsky model was therefore adopted. A complete description is given in [5]. The transitional character of the wall jet, albeit only within a few slot heights downstream of the discharge, made the use of Germano's dynamic Smagorinsky model more appropriate for this flow, yielding good agreement between the simulation and the experiments (see [3]).

3 Results

3.1 Preliminaries

A few results for mean-flow quantities and second moments are presented first, in order to convey a global view, but the emphasis is on budgets and structural features. For the back-step flow, properties are normalised by the step height h and the maximum velocity in the inlet channel U_c.

Results for the jet flows are given only at the far-field location, $x = 20b$. At this location both flows approach a state of self-similarity in the outer layer, with this state identified

through scaling the relevant flow variables with the maximum velocity, U_{max}, and the half-thickness, $y_{1/2}$ (the distance from the wall to the half-of-maximum-velocity point). Using this scaling, the outer layers of the two jets were observed to display insignificant streamwise variations beyond $x/b \sim 14$.

3.2 The mean flow and the turbulence properties

Figures 4-11 present profiles of the mean-velocity and Reynolds shear stress for all three flows considered. For the back-step flow, the profiles are given at two locations ahead of the reattachment location ($x_r = 7h$) and one well downstream, in the recovery region. The data are compared with two sets of experimental results, one by Yoshioka *et al.* [6] and the other by Kasagi *et al.* [10], as well as with the DNS results of Le *et al.* [11], the last two being for a Reynolds number of 5100 – that is, not far above the present value. The DNS data relate to a geometry that does not include an upper wall, but a zero-shear upper boundary condition. This difference is obviously reflected in results for the upper part of the domain for wall-normal distances well above the outer layer, $y/h > 2$, but is of little consequence to the region where the outer layer develops (around $y/h \sim 1$) and in the near-wall region, where comparisons show good agreement between the results. An exceptional feature is the high streamwise stress predicted by the present simulation at the upper wall. This reflects the fact that, at the lower Reynolds number pertaining to this simulation, the flow along this wall is incipiently separated, with separation occurring intermittently. It is also noted that Yoshioka *et al.* report a shorter reattachment length, $x_r = 5.5h$, than the present value of 7, this discrepancy being most likely due to 3D contamination in the experiments. This is an issue discussed in [5], where a complete comparison of the full turbulence statistics is also included.

A global view of the recovery region is conveyed in Fig. 9 by way of universal velocity profiles at 1.59 and 2.32 times the reattachment distance, x_r. The profiles demonstrate the slow recovery towards an equilibrium state, identified by the log law. The depressed velocity region, with roughly correct log slope, is the one in which the outer shear layer and the inner boundary layer interact strongly, and it will be shown latter that this region is characterised by a slow evolution towards the equilibrium state associated with the effects of the outer layer. The detailed mechanisms contributing to this slow recovery will also be discussed below by reference to the budgets and structural features.

For the real wall jet, extensive comparisons with the experiments are presented and discussed in [3], while a detailed discussion on the discrimination of wall-blocking effects from wall-shear effects is given in [7]. Here, profiles of mean velocity and Reynolds stresses in the (nearly) self-similar region are included in Figs. 10 and 11, respectively, to highlight some major differences between the two jets. Such differences arise from the non-vanishing values of the streamwise and wall-parallel stresses at the wall of the wall-shear-free jet. In the absence of wall shear, large eddies originating from the outer layer *impinge* on the wall without damping by viscous action, thus resulting in a high finite value of turbulence energy at the wall. The near-wall structural features of the two jets also differ greatly. In particular, the near-wall shear gives rise to small-scale, elongated eddies, while in the absence of shear, the eddies are more 'isotropic'. This implies different redistribution mechanisms of turbulence energy among the normal stresses in the near-wall region, discussed in more detail in [7].

3.3 Budgets

The selection of budgets included herein are intended to highlight features common to both wall jets and the back-step flow. For the former, budgets are reported for $x/b = 20$,

where the flow is close to being self-similar. For the latter, they are given for two locations, one at $x/h = 7$, close to the mean reattachment location, and the other well downstream of the reattachment point, at $x/h = 16$. The budgets at $x/h \leq 7$ were found to be very similar to the corresponding ones at other locations within the recirculation zone and, indeed, around the time-averaged reattachment location. This is illustrated by the comparison, in Fig 12, between the turbulence-energy budgets $x/h = 7$ and $x/h = 4$, which are seen to be closely similar. The preferential focus on the location $x/h = 7$ is motivated by the fact that the wall-shear vanishes at this location, a state corresponding to the zero-wall-shear jet. The terms included in the budgets are those constituting the transport equations that govern the evolution of the stresses:

$$\frac{\partial \overline{u_i u_j}}{\partial t} + \underbrace{\overline{U}_k \overline{u_i u_j}_{,k}}_{C_{ij}} = \underbrace{-\overline{u_k u_j} U_{i,k} - \overline{u_k u_i} \overline{U}_{j,k}}_{P_{ij}} + \underbrace{\nu \overline{u_i u_j}_{,kk}}_{D_\nu} \underbrace{-\overline{u_i u_j u_k}_{,k}}_{TTT_{ij}} \underbrace{-\frac{(\overline{u_i p_{,j}} + \overline{u_j p_{,i}})}{\rho}}_{\Pi_{ij}} + \underbrace{\varepsilon_{ij}}_{\text{dissipation}} \tag{1}$$

The turbulence-energy budget is deduced from the sum of the normal-stress equations. Here, we point out that the dissipation is deduced from the balance of Eq. (1), which implies that ε_{ij} represents the total level of dissipation, including the viscous and subgrid-scale contributions. While the latter also contains non-dissipative fragments, this contribution is insignificant. Indeed, the level of the subgrid-scale term as a whole is rather low in the present simulations. Thus, typically, the level of dissipation rate of the turbulence energy, evaluated from the exact definition, was found to be of order 50-70% of that determined from the imbalance, and both were observed to have very similar qualitative features.

The budgets for the turbulence energy are shown in Fig. 12. The main feature linking the reverse-flow ($x/h = 4$) and reattachment regions of the backward-facing step ($x/h = 7$) to the zero-wall-shear jet is the low near-wall shear production. At the reattachment, production is close to zero. With the near-wall shear being very small, it is observed that the main input of turbulence energy into the near-wall layer is caused by a high level of turbulent transport from the outer shear layer towards the wall, in particular in the respective interaction layers $0.05 < y/h < 0.25$ and $0.02 < y/y_{1/2} < 0.2$, although convection is also significant, because of the slip at the wall in the zero-wall-shear jet. Very near the wall, both energy budgets indicate a balance mainly between turbulent transport (combining triple correlation and pressure diffusion) and dissipation.

Downstream of reattachment, as the flow recovers, a new boundary layer develops, and mean-shear production close to the wall becomes a major contributor to the turbulence energy. Here, a balance qualitatively akin to that in a standard boundary layer is observed, wherein production is mainly balanced by dissipation in the near-wall region. However, a major difference relative to a standard boundary layer is the large input of energy by turbulent transport from the outer shear layer towards the wall, in particular in the interaction region ($0.15 < y/h < 0.3$). While in the reverse-flow zone, the turbulent transport provides the main input of energy, this process contributes at a level similar to production in the interaction region of the recovery region. This combined influence is also observed in the wall jet, although the contribution of diffusion is more pronounced, as the production is low in the interaction region ($0.08 < y/y_{1/2} < 0.25$).

Distributions of production-to-dissipation ratio and integral length-scales, given in Figs.

26-27, respectively, will be discussed later in some detail. However, it is useful to highlight here that these distributions demonstrate that the high input of turbulent transport from the outer shear layer towards the wall, in both the wall jet and the recovery region, results in strong departures from equilibrium in the interaction regions – stronger in the wall jet than in the back-step flow, because production is lower in the former than in the latter. Nevertheless, it is this process that is mainly responsible for the strong departures from the log law, observed earlier in Fig. 9.

Budgets for the shear stress are presented in Fig. 13. All show significant levels of transport by triple correlations in the near-wall region. However, in the back-step flow, this transport is negative, while it is positive in both jet flows, this difference being associated with the opposite signs in the respective strain rates (see Figs. 4 and 10). Both in the recirculation region of the back-step flow and in the zero-wall-shear jet, the production is low, and the main balance occurs between turbulent transport and pressure-velocity correlation. On the other hand, in the back-step recovery region and in the real wall jet, production is high, and this is counterbalanced mainly by pressure-velocity correlation. However, the contribution of transport by triple correlations is still significant.

Of the normal-stress budgets, those for the wall-normal component are the most interesting and informative, because the wall-normal intensity is intimately linked to the shear stress. On the whole, the budgets of $\overline{uu}$ are similar to those of the turbulence energy, and the budgets of $\overline{ww}$ do not differ greatly among the three flows examined herein, all being broadly similar to those found in a standard boundary layer.

Figures 14 shows that the budgets for the back-step flow, within the separation region and in the recovering wake, have features similar to those of the zero-wall-shear and the real wall jets, respectively. Thus, the pair of budgets on the left-hand side of Fig. 14 both feature a high level of transport by triple correlations from the outer layer towards the wall, which is compensated by a high negative contribution of the pressure-velocity correlation in the near-wall region, this latter contribution being, in absolute terms, higher than dissipation. However, in the back-step flow, dissipation tends to become more important as the flow recovers. As regards the budget for real wall jet, the stress $\overline{vv}$ is also elevated by a large gain through turbulent transport, but a lower and slightly negative pressure-velocity correlation arises near the wall, the dissipation being here the dominant process. It is important to point out that the $\overline{vv}$ budgets for both the back-step flow in the recovery region and the real wall jet differ strongly from that for a standard boundary layer, in which turbulent transport is low, the main balance being between a large gain by pressure-velocity correlation and loss by dissipation in the near-wall region. This implies that the large gain of turbulent transport modifies the energy-redistribution process in the present wall flows, when compared to a standard boundary layer. Further details will be given below by reference the non-deviatoric part of the velocity-pressure correlation. It is finally noted here that Kuroda *et al.*[12] also reported a prominence of turbulent transport in the budgets of the Reynolds stresses in their DNS of a channel, in which the wall-shear stress on one wall is much lower that that on the other wall, resulting in a turbulent Couette-Poiseuille flow. Turbulent transport is even more pronounced in the present flow, because of the presence of the outer shear layer.

3.4 The near-wall flow structure

The budgets presented in the previous section brought to light some significant similarities between the processes in two disparate regions in the back-step flow and those in the two wall jets examined. As shown in the present section, these similarities may be associated with corresponding structural features in the wall region of the flows considered.

The instantaneous contours of the streamwise-velocity fluctuations represented on Fig.

15 suggest a very different wall structure between the reverse-flow region and the recovery region of the backstep flow. As the flow recovers, the near-wall structure, here visualized by way of contours of streamwise-velocity fluctuations, is dominated by "streaky", fine and elongated features, which are characteristic of alternate high- and low-speed streamwise fluctuations. In contrast, in the reverse-flow region, close to the nominal reattachment location, the contours indicate a far more "isotropic" structure. Figure 16 shows that the corresponding near-wall structure of the zero-wall-shear jet is, likewise, characterised by rounded rather than streaky features. This commonality reflects the fact that the dominant near-wall mechanism in both flows is the "splatting" of eddies originating from the outer flow onto the wall without preferential wall-parallel orientation. For the wall jet, the details of the process are discussed extensively in [7]. Here, they are illustrated by instantaneous fields of contours of the velocity-fluctuation vector $(v/U_o, w/Uo)$, given in the upper plot of Fig. 17, across a wall-normal (y, z) plane just upstream the reattachment location, in comparison with a corresponding upper plot in Fig. 18 for the self-similar region of the zero-wall-shear jet. Both fields exhibit a pattern that indicates large-scale eddies originating from the outer layer, migrating towards the wall and then impinging upon it. In the case of the zero-wall-shear jet, viscous effects are negligible, and the intensity of "splatting" is high. In the back-step flow, on the other hand, the imposition of zero slip at the wall introduces some measure of viscous damping, but the dominance of splatting is nevertheless evident, and impinging motions of large eddies originating from the outer layer penetrate up to the wall, as is evident from the upper plot in Fig. 17.

Downstream of reattachment, the flow recovers, and the wall shear increases progressively. Thus, here, the strained near-wall layer partially insulates the wall from splatting, and the near-wall layer is characterized by a streaky structure with splatting damped, as seen from Figs. 15 and 17 (lower plots). Similar characteristics are observed in the real wall jet, as shown in the lower plot of Fig. 18.

Specifically in respect of the streaky layer, it is interesting to refer here to DNS studies by Lam and Banarjee [8] who have shown that the formation of streaks is not tied primarily to the presence of the physical wall itself, but is a consequence of high shear. In their numerical experiments they imposed a mean shear onto a free-slip surface and observed the formation of streaks for sufficiently high shear even without a wall. At low shear, however, no streaks form in the surface layer or near a wall. Lam and Banarjee further identify the non-dimensional strain, $\tilde{S} = \frac{\overline{uv}S}{\varepsilon}$ $(S = \frac{\partial U}{\partial y})$ as the parameter governing the formation of streaks. They show that streaks can form when $\tilde{S} \geq 1$, and that, the higher the parameter $\tilde{S}$ is, the more pronounced the streaks are. To investigate this dependence, Fig. 19 presents several profiles of $\tilde{S}$, namely three from the present back-step-flow simulations, at $x/h = 4, 10$ and 15, two from Le *et al.*'s DNS for a similar back-step flow, at $x/h = 10$ and 19, and two profiles (from the present computations and the DNS) in the channel upstream of the step, in which the flow is fully-developed. Inside the recirculation region, at the location $x/h = 4$, the parameter has a negative value because the shear stress and shear strain are de-correlated through the strong effects of other strains on the shear stress. The negative turbulence-energy production in this region (see Fig. 12) is also a reflection of this de-correlation. However, the magnitude of $\tilde{S}$, arguable the appropriate quantity to consider, is well below 1, which is compatible and consistent with the absence of streaks in this region (see top plot in Fig. 15). Following reattachment and recovery over approximately 3 step heights, the peak $\tilde{S}$, associated with the maximum mean-shear production, rises towards and exceeds 1, and this leads to the formation of the streaky structure at around $x/h \geq 10$, as shown in Fig. 15. However, comparison with the channel-flow variations shows that $\tilde{S}$ rises only slowly, and that its value at $x/h = 15$ is still considerably smaller than the level in the channel flow. Indeed, in the DNS of Le

et al., $\tilde{S}$ hardly rises at all between x/h=15 and 19. This is, again, a facet of the slow recovery of the post-reattachment flow and the response of the near-wall layer to shear in the presence of the influence of the outer layer. The maximum value $\tilde{S} > 2$ is found to arise in the wall jet, and this higher value is indeed associated with a more pronounced streaky wall structure, as illustrated by the contrasting structures in the lower plots in Figs. 15 and Fig. 16. For this flow, the present authors (see [7]) have shown that the thin wall layer, where the streaks form, is robust and acts as a "shield" which protects the wall itself from the large eddies impinging upon it. This feature was shown to be instrumental in the damping of the fluctuations as the wall is approached, and to result in a redistribution process of turbulence energy very different from the zero-wall-shear jet.

In the following section, the wall-limit behaviour of the turbulent fields is discussed by reference to the level of near-wall anisotropy and the redistribution of turbulence energy among the normal stresses through the pressure strain process.

3.5 Anisotropy and redistribution of energy

Scalar measures indicative of the level of the anisotropy are the second and third anisotropy invariants, $II = b_{ij}b_{ji}$ and $III = b_{ij}b_{jk}b_{kj}$, respectively, in which $b_{ij} = \overline{u_iu_j}/k - 2/3\delta_{ij}$ is the anisotropy tensor (see Fig. 20). A third interesting invariant, derived from those above, is Lumley's flatness parameter $A = 1 - 9/8(II - III)$. This parameter varies between the limits of 0, indicating two-component turbulence (at a wall or sharp interface), and 1, indicating isotropy. The variation of this parameter is especially pertinent in the context of turbulence modelling, as it is often used to procure the appropriate sensitivity of the pressure-strain approximation and dissipation equation to the proximity of the wall.

Prior to an examination of the above invariants, it is instructive to consider the normal components of the anisotropy tensor, b_{ii}, and this is done in Fig. 20. A point to note first is that the main distinction between the two wall jets relates to b_{11} and b_{33}. In both cases (indeed, at any wall), b_{22} must approach -1/3, as the wall-normal intensity vanishes. In the wall-shear-free jet, the wall-parallel anisotropy components at the wall are very similar; it is only away from the wall where b_{11} is substantially higher, due to wall-shear production. When a wall is introduced, b_{11} rises steeply close to the wall, and b_{33} drops correspondingly, suggesting substantially different energy-redistribution processes in the two flows. Corresponding differences are seen when comparing the distributions of the anisotropy components in the two regions of interest in the back-step flow. Around and ahead of the reattachment point, b_{11} and b_{33} are similar close to the wall. As wall shear becomes influential in the recovery region, these same components diverge in the same manner as they do in the wall jets. These common features are reflected by corresponding similarities in the behaviour of A considered next.

Fig. 21 contrasts profiles of A for the back-step flow at four locations against those derived for the two wall jets. As expected, all profiles asymptote to zero at the wall, indicating an approach to the two-component limit. In both the wall-shear-free jet and upstream of the reattachment location in the back-step flow, A remains high close to the wall, and then drops steeply towards zero. This suggests that the damping of wall-normal fluctuations occurs closer to the wall when wall shear is low. In contrast, as the back-step flow recovers, the near-wall anisotropy increases, due to the increasing viscous wall-shear effects, leading to a earlier damping of the stresses. This feature is also observed when wall shear is introduced to the wall jet. It is also interesting to compare the profiles of A in the recovery region of the back-step flow with those for the channel flow and the self-similar region of the real wall jet, and this is done in Fig. 22 in terms of wall scaling (note that no such comparison is possible for the zero-wall-shear jet, and this is the reason for using outer

scaling in the previous figure). These profiles bring to light the high near-wall anisotropy of the wall jet, relative to the recovery region, and also, more moderately, relative to the channel flow. This is consistent with the higher level of $\tilde{S}$ in the wall jet, seen in Fig. 19, indicating high strain and high shear production. Fig. 22 shows that the level of anisotropy in the back-step flow is still far lower than that in the real jet as well as the equilibrium channel boundary layer, and this reflects the weaker resistance to the penetration of the impinging motions from the outer layer, when compared to the real wall jet of the wall structure of the recovery region. This observation provides, on the one hand, some insight into the mechanisms inhibiting a recovery towards equilibrium, and is consistent, on the other hand, with the high negative near-wall peak of the velocity-pressure correlation of the normal stress $\overline{vv}$ needed to balance the high input of turbulent transport in the absence of strong near-wall shear. Thus, the relatively low level of $\tilde{S}$ inhibits the near-wall damping of velocity fluctuations, leading to higher level of near-wall flatness parameter and more vigorous near-wall motions and pressure fluctuations.

As will be seen below, one encouraging observation emerging from Fig. 21 and Fig. 25 is that A is well correlated with the wall-normal, non-deviatoric pressure-velocity correlation, Φ_{vv}, regardless of whether or not the near-wall flow is sheared. Thus, A appears to be a good indicator of the damping imparted to the wall-normal stress. On the other hand, the very different behaviour of the pressure-strain term, responsible of the redistribution of turbulence energy among the normal stresses and examined below, and also of the anisotropy of the dissipation, observed in the turbulence-energy budgets (see Fig. 12), calls into question the usefulness of A as the *only* parameter representing the effect of wall proximity in models for Φ_{ij} and ε_{ij}.

A more differentiated view of the anisotropy than that conveyed by A is provided by so-called anisotropy maps, which co-relate the second and third anisotropy invariants, II and III, respectively. Such maps are included in Figs. 23 and 24. Lumley has shown that any realisable state within any turbulent flow must fall within the triangular region. The loci shown within the realisability maps identify traverses across the flows in question, starting from the lower wall and progressing upwards in the direction of the arrows along the loci. Free shear layers are known to exhibit loci that are broadly aligned with the lower, left-hand line of the triangular domain, characterising "axisymmetric expansion". This is a behaviour returned by the zero-wall-shear jet and also by the lower near-wall layer of the back-step flow at $x/h = 7$ (as well as at $x/h = 4$, not included here). At the wall, turbulence tend to a two-component state, as $\overline{vv}$ declines rapidly. This state is identified by the upper side of the triangle. In the presence of wall shear, there is a tendency for II and III to move upwards, broadly parallel to the lower right-hand line of the triangle. This is a behaviour characteristic of near-wall shear. In fact, in a conventional boundary layer, the state of anisotropy in the log-law region is characterised by a locus hugging the lower right-hand-side line. The real wall jet features a thin near-wall region that is akin to a log-law layer. However, the mean-velocity profile for the wall jet, reported in Dejoan and Leschziner [3], shows that this log layer is thin and indistinct, reflecting the strong influence of the outer shear layer on the near-wall region. A qualitatively similar behaviour is observed in the lower near-wall layer of the back-step flow at x/h=15. Again, there is a tendency for the locus to rise, but clearly the anisotropy state in this layer is far from that of an equilibrium layer (or indeed the upper-wall layer).

A process that plays a particularly important role in relation to anisotropy is the pressure-velocity interaction Π_{ij}. This term is conventionally split into two fragments, $\Pi_{ij} = \Phi_{ij} + d_{ij}$, where $\Phi_{ij} = \overline{\frac{p}{\rho}\left(u_{i,j} + u_{j,i}\right)}$ corresponds to the pressure-strain term and $d_{ij} = -\overline{\frac{p}{\rho}(u_i\delta_{kj} + u_j\delta_{ki})}_{,k}$, to the pressure diffusion term. The pressure-strain term, Φ_{ij}, is trace-free and thus responsible for the redistribution of the energy among the normal-

stress components. This term is not only highly influential, but is one that presents major challenges to closure at second-moment level. It is therefore of considerable interest herein.

Against this background, Figure 25 shows profiles of the pressure-strain components relating to the normal stresses. One particularly interesting feature, linking the present considerations to the earlier discussion of b_{ij}, is the similarity of the energy-redistribution processes in the recirculation region and the zero-wall-shear jet. In both cases, this redistribution is from $\overline{vv}$ to both $\overline{uu}$ and $\overline{ww}$. As the separated flow recovers, the energy-redistribution process becomes similar to the real wall jet, wherein the energy is transferred from $\overline{vv}$ and from $\overline{uu}$ to $\overline{ww}$. Again, this links well with the previous observations on the behaviour of b_{ij}. In the latter case, a high level of $\overline{uu}$ is produced by the near-wall shear, and energy has to be removed from $\overline{uu}$, so that all stresses are made to vanish at the wall (see [7] for more details). A point of difference between the wall jet and the recovery region lies in the near-wall variation of Φ_{uu}. Specifically, this components features a distinct negative peak in the case of the wall jet, while this feature is absent in the recovery region of the back-step flow. This is likely to be linked to corresponding differences in the level of $\tilde{S}$, which is significantly higher in the wall jet, thus resulting in a higher generation that needs to be compensated by an elevation of Φ_{uu}.

The similarities highlighted above suggest strongly that wall-blocking effects dominate over wall-shear effects inside the recirculation region of the back-step flow. In contrast, as the flow recovers, wall-shear effects exert a much greater influence, although the effects are not as strong as observed in the wall jet. As demonstrated by the present authors [7], the energy-redistribution in the wall jets is closely linked to structural features near the wall – in particular, the "splatting" of large-scale eddies onto the wall and the shielding and damping effected by the near-wall shear layer.

3.6 Length scale and equilibrium

It is of interest to examine the near-wall variations of the integral length scale $k^{3/2}/\varepsilon$, normalised by the equilibrium length scale $C_\mu^{-3/4}\kappa y$, as these indicate, alongside variations of the production-to-dissipation ratio, P/ε, departures from local equilibrium. Such profiles are given on Fig. 26. In the back-step flow, as the outer layer develops, the length scale increases in the wall region of the recirculation zone. In the reattachment region, $x/h = 7$, where the outer layer interacts especially strongly with the wall, the length scale close to the wall reaches a maximum value and then diminishes as the flow recovers and a near-wall layer forms. A high value for the integral length scale is also observed in the zero-wall-shear jet, relative to the real wall jet, and this reflects the presence of intense, large-scale outer-layer motions towards the wall, which are not damped by viscous and shear-induced effects. Very close to the wall, the steep rise in the normalised length scale is, for this flow, rather misleading, because the length scale itself remains finite at zero shear, while y declines to zero. In the case of the back-step flow, at $x/h = 7$, the length scale vanishes at the wall, but is nevertheless substantially elevated in this region relative to the values downstream, suggesting a material influence of the outer layer in this region, similar to that observed in the zero-wall-shear jet. As the flow recovers, shear and viscous effects become influential, and these tend to reduce the integral length scale, with the near-wall eddies changing their structure to become elongated and smaller in size. However, even at $x/h = 15$, the normalised near-wall length scale is substantially above unity, and this suggests that outer-layer turbulence continues to significantly affect the boundary layer in the recovery region. Previous studies (see Hasan, [13]) have indeed revealed that the large scale structures issuing from the outer layer tend to persist well downstream of reattachment.

As seen in Fig. 26, the length scale within the reverse-flow layer, at $x/h = 4$, is

substantially lower than that $x/h = 7$ and also 15. This is rather surprising, at first sight, because all previous comparisons and considerations demonstrated a high degree of commonality between the conditions at $x/h = 7$ and 4 (and thus also with the zero-wall-shear jet). It is recalled, in particular, that the two locations share a low value of near-wall $\tilde{S}$, which signifies the absence of a streaky near-wall layer that shields the wall from the outer scales. In the case of the reverse-flow region, the shear layer above the thin backward-moving boundary layer has a highly complex structure, as a consequence of impingement, strong curvature and recirculation. This is signified, for example, by the negative turbulence-energy production and negative $\tilde{S}$ in this region. Hence, it is difficult to fully interpret the interaction between the outer layer and the near-wall region within the recirculation zone. The fact that the length scale is rather low in this region may be linked to the negative production, which tends to lower k and hence l_ϵ. On the other hand, the near-wall peak at around y/h=0.05, indicates that turbulence is transported from the outer layer towards the near-wall region (see Fig. 12). In structural terms, the length scale of the turbulent motions in the recirculation zone are lower than at reattachment, because the vortical structures transported into this zone by the reverse motions originate from 'young' portions of the free shear layer above it, and these are relatively small. As they are transported towards the wall, they are subjected to splatting, and the fact that $\overline{ww} > \overline{uu}$ in this region, as seen upon comparing Figs. 5 and 7, is a clear indicator to this process, which tends to reduce the length scale further. Finally, in general, the residence time of eddies in the recirculation zone is especially high, and this encourages eddy break-up and a reduction in length scale. Thus, although it might appear that the flow at this position is closer to equilibrium than in the other two, the reserve is, in fact, the case, as is well brought out by the distributions of the production-to-dissipation ratio shown in Fig. 27. These distributions demonstrate strong departures from local equilibrium in both the recirculation and impingement regions and immediately downstream of it, due to a combination of low (or negative) production and gain by turbulent transport. A similar behaviour, for identical reasons, is displayed by the zero-wall-shear jet. As the back-step flow recovers, the near-wall peak of the ratio P/ε increases and eventually exceeds unity. Thus here, the near-wall flow does not appear to be far from a state of equilibrium. However, as shown earlier by reference to the parameter $\tilde{S}$ (which, in the near-wall region, is equivalent to the ratio P/ε – see section 3.4), recovery is actually very slow, and at the farthest downstream location included in the simulation, the near-wall region has not reached the level of anisotropy equivalent to that of a fully-developed channel flow. A partial explanation for this apparent inconsistency is provided by the budget of turbulence energy, Fig. 14. For $x/h = 16$, it is observed that convection and diffusion broadly compensate each other, so that an approximate balance between production and dissipation is returned above the viscous sublayer.

In the interaction region of the real jet, it is the vanishing shear production, associated with a reversal in the shear strain, that leads to the much lower level of the production-to-dissipation ratio, relative to that observed in the recovery region of the back-step flow.

4 Conclusions

The present study has demonstrated, mainly by reference to budgets, anisotropy parameters and near-wall structural properties, that turbulence mechanisms effective in different regions of a separated flow relate to those in two wall jets, one evolving along a real wall and the other along a zero-shear slip boundary. The latter jet only includes wall-blocking effects in its near-wall region, while the former combines wall-blocking with near-wall shear effects. An interesting finding is the similarity between the near-wall regions

in the impingement and recirculation zone of the back-step flow and the zero-wall-shear jet, which suggests a predominance of wall-blocking effects inside the recirculation zone. In this region, mean-shear production is low, and the main contributor is transport by triple correlations from the free shear layer towards the wall, which is counterbalanced by the pressure-velocity-correlation terms. In the near-wall layer of the back-step recovery region, mean-shear production becomes predominant, and the budgets for the back-step flow contain features that are close those in the corresponding budgets for the wall jet. In particular, transport by triple correlation is important, especially in the interaction region. In fact, in all flow regions considered herein, the turbulent transport provides a significant, if not major, input of energy into the wall-normal stress, a process that is compensated by pressure-velocity correlation and dissipation. This type of interaction differs substantially from that in standard near-wall flows close to equilibrium, for which the wall-normal stress is mainly governed by pressure-velocity correlation and dissipation, the transport by triple correlation being small.

The redistribution of the turbulence energy among the normal stresses through the pressure-strain process reinforces the similarities between, on the one hand, the reverse-flow layer and the zero-wall-shear jet, in which energy is transferred from the wall-normal component to the both wall-parallel components, and, on the other hand, between the post-reattachment recovery region and the real jet, in which shear-produced energy has to be removed from the streamwise-stress component to the spanwise component. The above different energy-redistribution scenarios, applicable to the recirculation and the post-reattachment recovery regions of the back-step flow, suggest that the importance of wall-blocking effects depends strongly on the streamwise evolution and local structure of the flow, a fact that presents a significant challenge to statistical closures, second-moment models in particular.

The correspondence in the statistical properties identified for the respective flows examined herein have been found to go hand-in-hand with close similarities in structural features in the respective near-wall layers. In the presence of strong shear, a streaky structure arises, while weak or no shear leads to a more "isotropic" structure. The former is associated with the formation of a shear layer that shields the wall from large eddies that migrate towards or impinge onto the wall the process that predominates in weak shear. The non-dimensional parameter, $\tilde{S} = \frac{\overline{uv}S}{\varepsilon}$, previously shown to characterize the effects of shear on the near-wall structure in fully-developed flows, also appears to govern the formation of near-wall streaks in the present flows. For values well below unity, no streaky structure arises, and this has been shown to be so in the zero-wall-shear jet and in the recirculation zone of the back-step flow. On the other hand, values above unity arise in the real wall jet and in the recovery region of the back-step flow, and in both cases, the near-wall structure is distinctly streaky. The connection between the wall structure and the wall-blocking/near-wall-shear effects presented herein suggests that the parameter $\tilde{S}$ can also be viewed as a good indicator of the nature of the energy-redistribution process occurring in different types of wall-bounded regions.

Acknowledgements

This study was supported financially by the UK Science and Engineering Research Council (EPSRC). The computations were performed on the Origin 3800 computer at the national CSAR service in Manchester, using resources provided as part of the EPSRC grant.

References

[1] Jang Y-J., Leschziner M. A., Abe K. and Temmerman L., 2002, Investigation of anisotropy-resolving turbulence models by reference to highly-resolved LES data for separated flow. *Flow, Turbulence and Combustion,* **69**, 161–203

[2] Wang C., Jang Y-J. and Leschziner M. A., 2004, Modelling two- and three-dimensional separation from curved surfaces with anisotropy-resolving turbulence closures. *Int. J. Heat and Fluid Flow,* **25**, 499–512

[3] Dejoan A. and Leschziner M. A., 2005, Large eddy simulation of a plane turbulent wall jet. *Phys. Fluids,* **17(2)**, 025102

[4] Dejoan A., C. Wang and Leschziner M. A., 2005, Assessment of turbulence models for predicting the interaction region in a wall jet by reference to LES solution and budgets. Proc. ETMM6, Sardinia, May 23–25, Proc. 97–106

[5] Dejoan A. and Leschziner M. A., 2004, Large eddy simulation of periodically perturbed separated flow over a backward-facing step. *Int. J. Heat and Fluid Flow,* **25**, 581–592

[6] Yoshioka S., Obi S. and Masuda S., 2001, Turbulence statistics of periodically perturbed separated flow over a backward-facing step. *Int. J. Heat and Fluid Flow,* **22**, 393–401

[7] Dejoan A. and Leschziner M. A., 2005, Separating the effects of wall-blocking and near-wall shear in the interaction between the wall and the free-shear layer in a wall jet. *Phys. Fluids* **18 (6)**,065110

[8] Lam k. and Banarjee K., 1992, On the condition of streak formation in bounded turbulent flow. *Phys. Fluids,* **A 4**(2), 306–320

[9] Eriksson J. G., Karlsson R. I. and Persson J., 1998, An experimental study of a two-dimensional plane turbulent wall jet. *Expt. in Fluids,* **25**, 50–60

[10] Kasagi N. and Matsunaga A., 1995, Three-dimensional particle-tracking velocimetry measurement of turbulence statistics and energy budget in a backward-facing step flow. *Int. J. Heat and Fluid Flow,* **16**, 477–485

[11] Le H., Moin P. and Kim J., 1997, Direct simulation of turbulent flow over a backward-facing step flow. *J. Fluid Mech.,* **342**, 119–139

[12] Kuroda A., Kasagi N. and Hirata M., 1993, Direct numerical simulation of turbulent plane Couette-Poiseuille flows: effect of mean shear on the near wall turbulence structures. Ninth Symposium on "Turbulent shear flows", Kioto, Japan, August 16-18, **8**, 4-1–4-6

[13] Hasan M. A. Z., 1992, The flow over a backward-facing step under controlled perturbation: laminar separation. *J. Fluid Mech.,* **238**, 73–96

List of Tables

List of Figures

Flow	Reynolds number	Domain size	Grid
backward-facing-step	3700	inlet channel: $4h \times 2h \times 4\pi/3h$ dowsntream of the step: $18h \times 3h \times 4\pi/3h$	$160 \times 64 \times 64$ $160 \times 128 \times 64$
wall jet	9600	$22b \times 10b \times 5.5b$	$420 \times 208 \times 96$
zero-wall-shear jet	9600	$22b \times 10b \times 5.5b$	$420 \times 208 \times 96$

Table 1: Flow conditions and numerical parameters

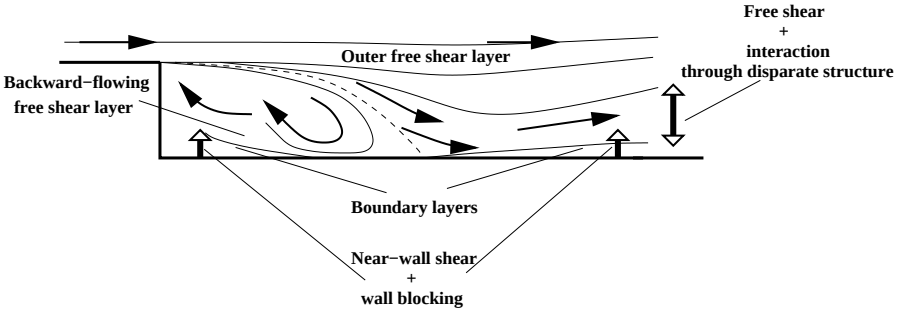

Figure 1: Shematic of major flow components of interest and interactions among them in the backward-facing-step flow.

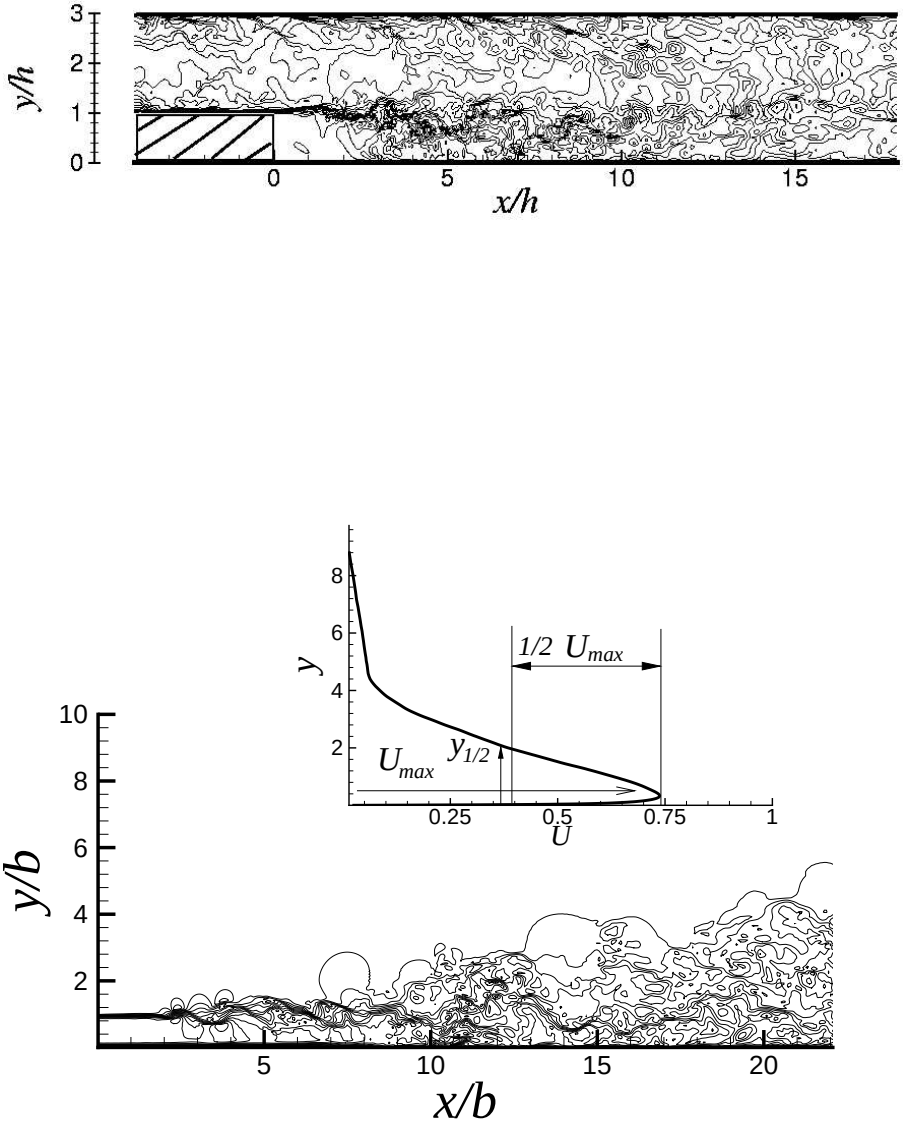

Figure 2: The flow configurations under consideration

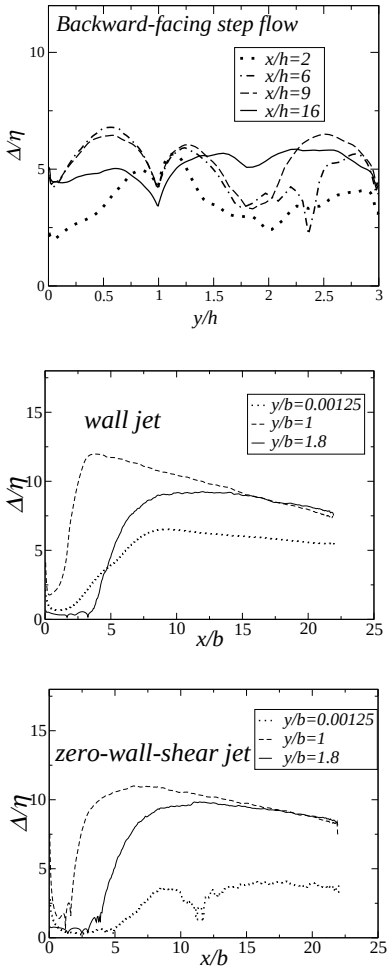

Figure 3: Ratio of the cell size to the Kolmogorov length scale along various grid lines

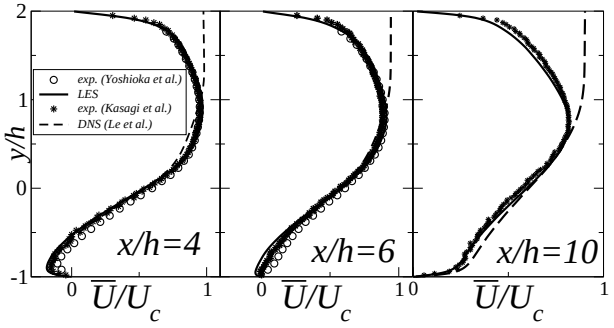

Figure 4: Backward-facing-step flow: profiles of the streamwise velocity

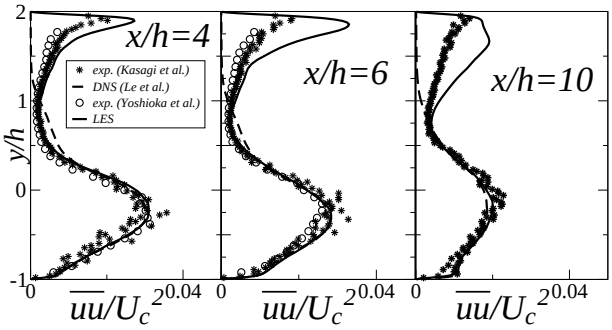

Figure 5: Backward-facing-step flow: profiles of the streamwise Reynolds stress

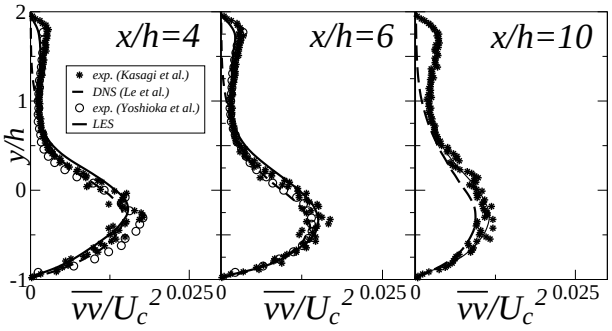

Figure 6: Backward-facing-step flow: profiles of the wall-normal Reynolds stress

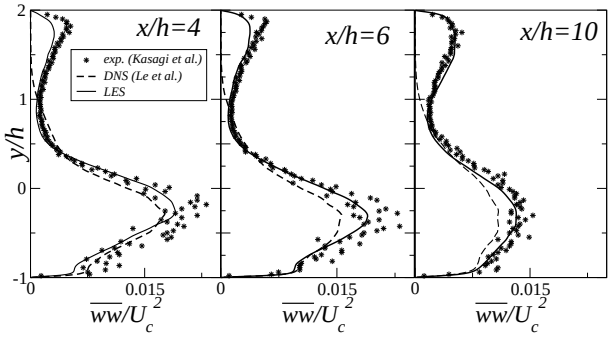

Figure 7: Backward-facing-step flow: profiles of the spanwise Reynolds stress

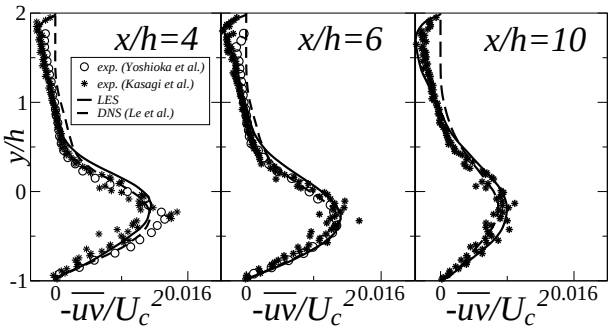

Figure 8: Backward-facing-step flow: profiles of the Reynolds shear stress

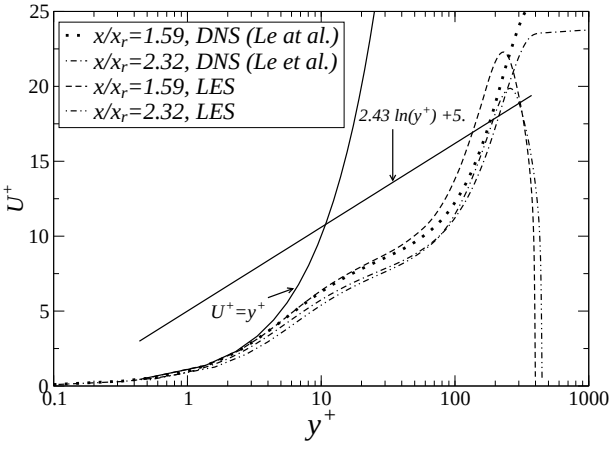

Figure 9: Backward-facing-step flow: universal velocity profiles

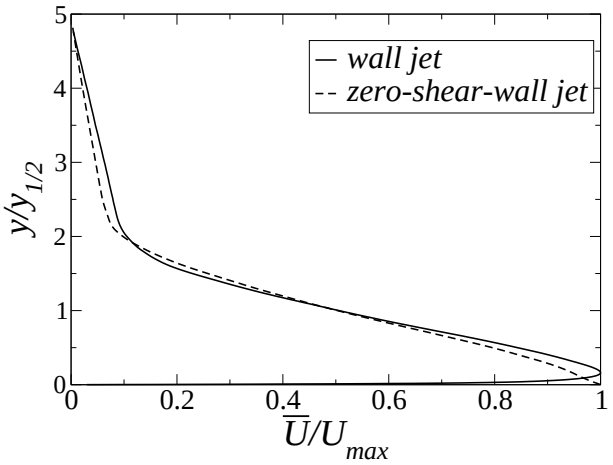

Figure 10: Wall and zero-wall-shear jets: profiles of the streamwise velocity

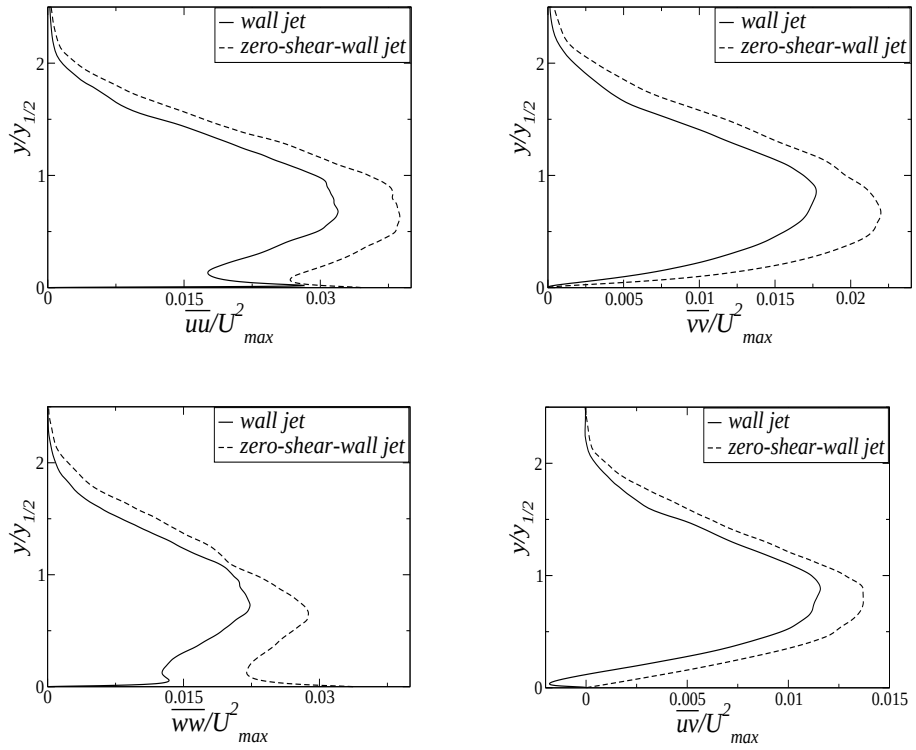

Figure 11: Wall and zero-wall-shear jets: profiles of the Reynolds stresses

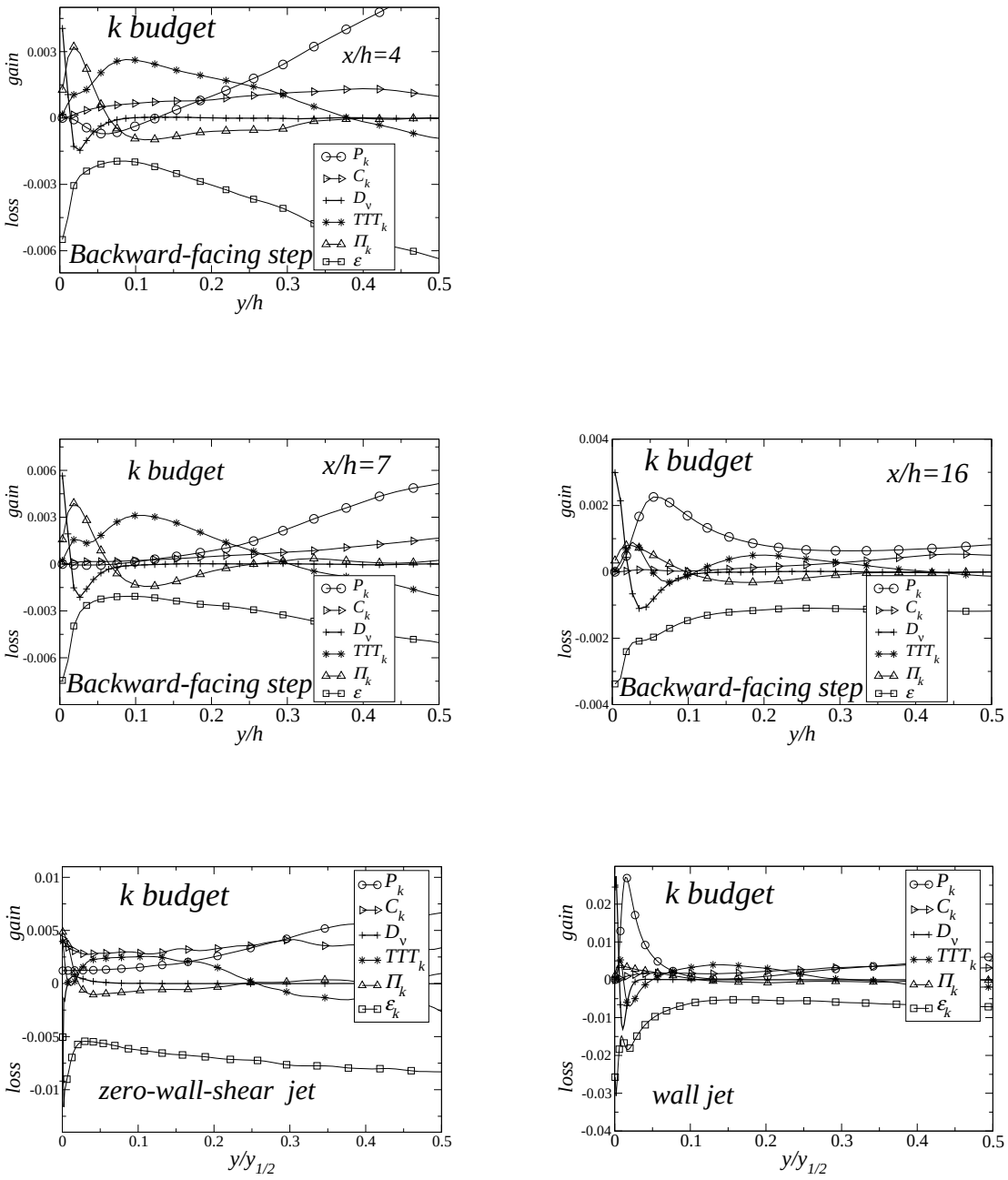

Figure 12: Budgets of the turbulence energy : P_k: production; C_k: convection; D_ν: viscous diffusion; TTT_k: transport by Triple correlations; Π_k: velocity-pressure correlations (identical to pressure diffusion for k); ε: dissipation. See Eq. (1) for definition of budget terms

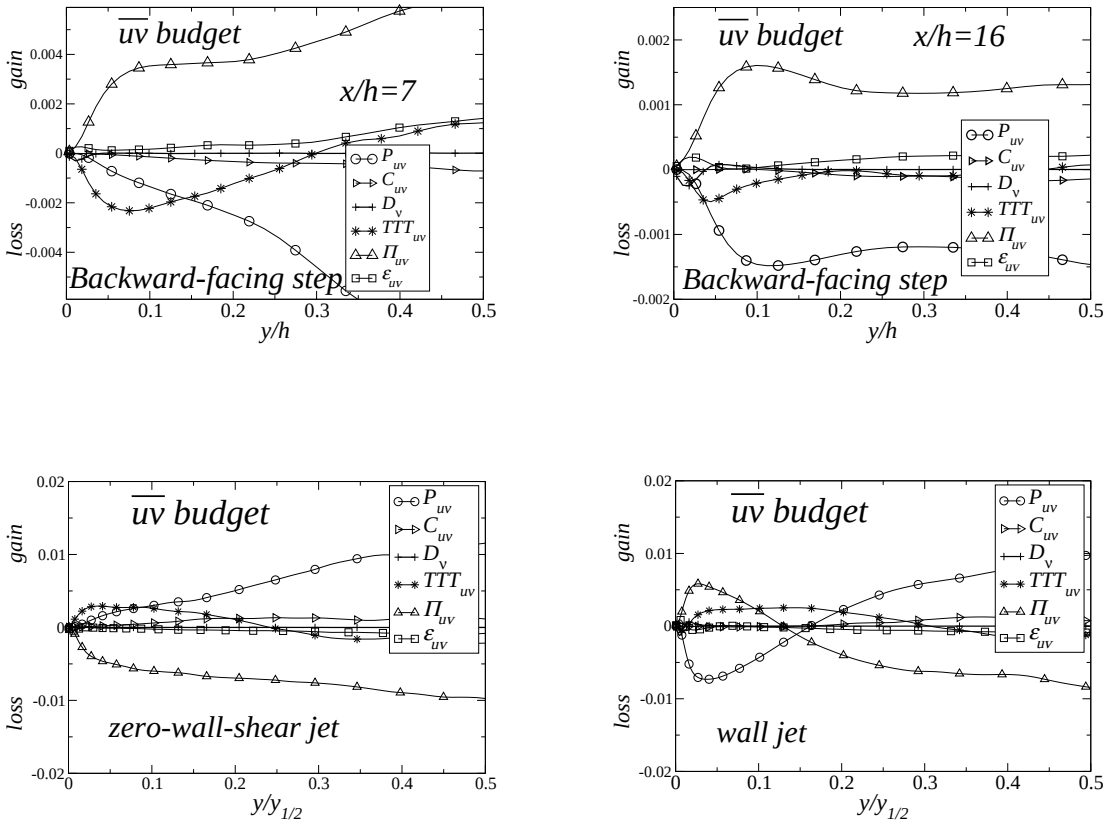

Figure 13: Budgets of the shear stress: P_{uv}: production; C_{uv}: convection; D_ν: viscous diffusion; TTT_{uv}: transport by Triple correlations; Π_{uv}: velocity-pressure correlations; ε_{uv}: dissipation. See Eq. (1) for definition of budget terms

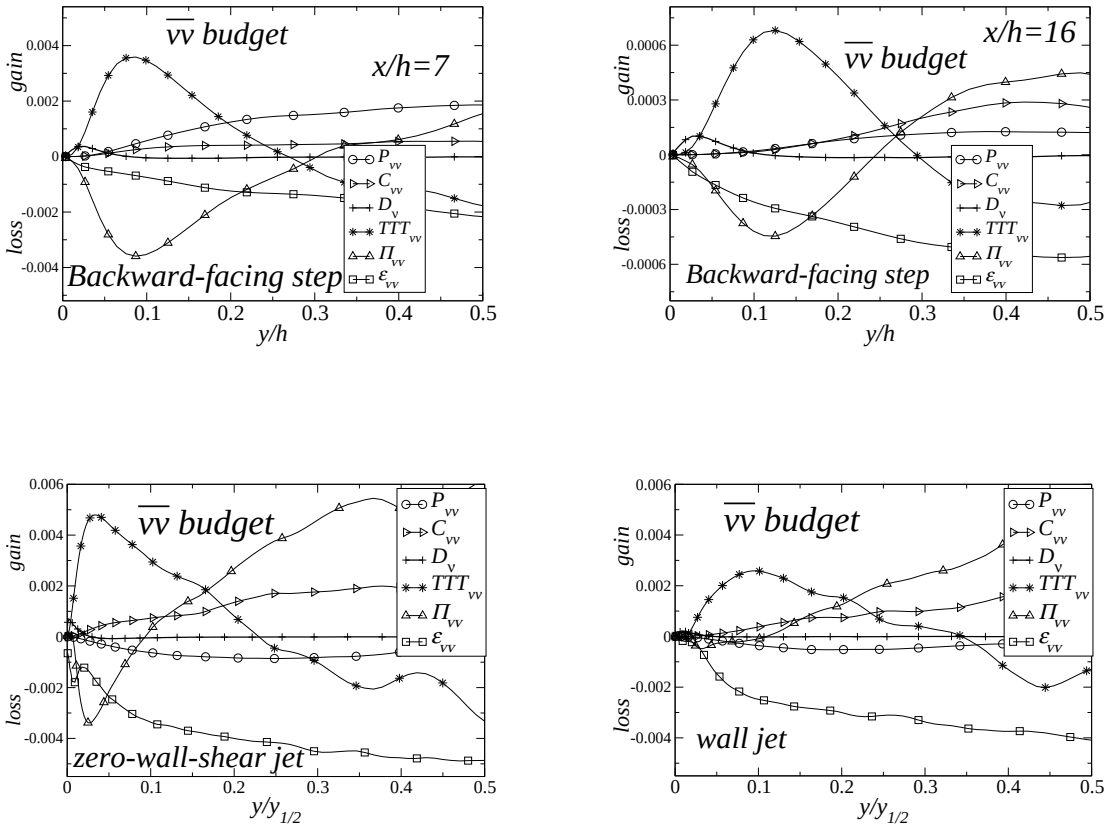

Figure 14: Budgets of the wall-normal stress: P_{vv}: production; C_{vv}: convection; D_ν: viscous diffusion; TTT_{vv}: transport by Triple correlations; Π_{vv}: velocity-pressure correlations; ε_{vv}: dissipation. See Eq. (1) for definition of budget terms

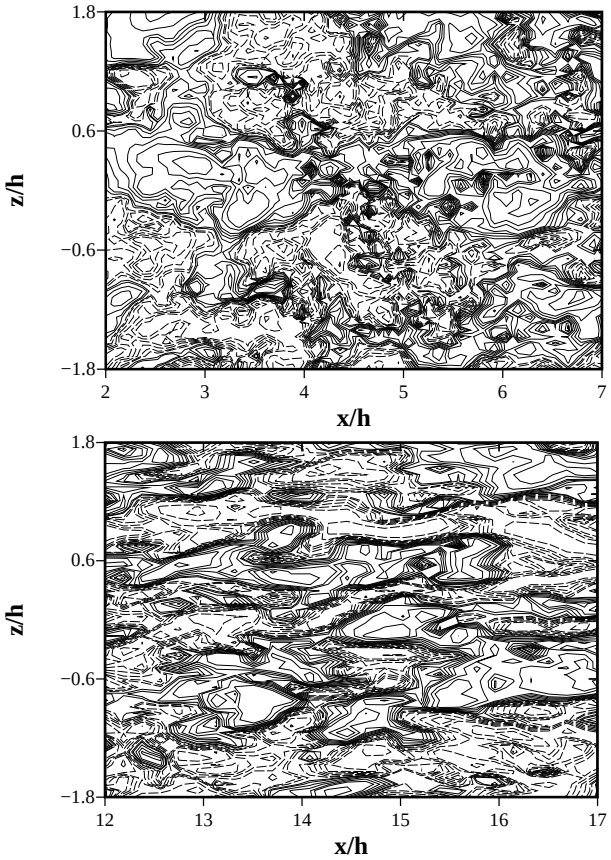

Figure 15: Backward-facing-step: contours of instantaneous streamwise-velocity fluctuations, u/U_o, parallel to the wall at $y/h \sim 0.007$. The plot contains 40 contours of u/U_o values contained in the range [-1.5:1.5]. Upper plot: $2 < x/h < 7$. Lower plot: $12 < x/h < 17$

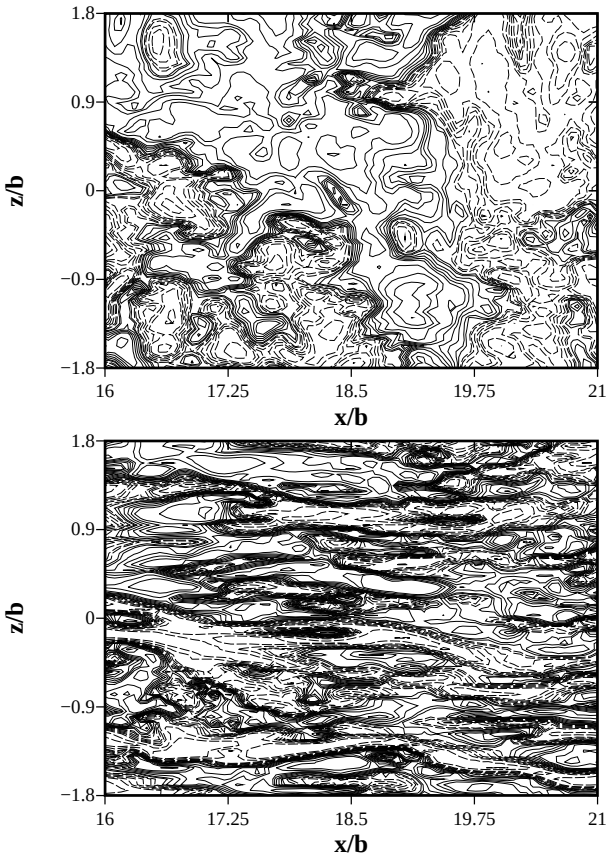

Figure 16: Jet flows: contours of instantaneous streamwise-velocity fluctuations, u/U_o, parallel to the wall at $y/y_{1/2} \sim 0.02$. The plot contains 40 contours of u/U_o values contained in the range [-1.5:1.5]. Upper plot: zero-wall-shear jet. Lower plot: real wall jet

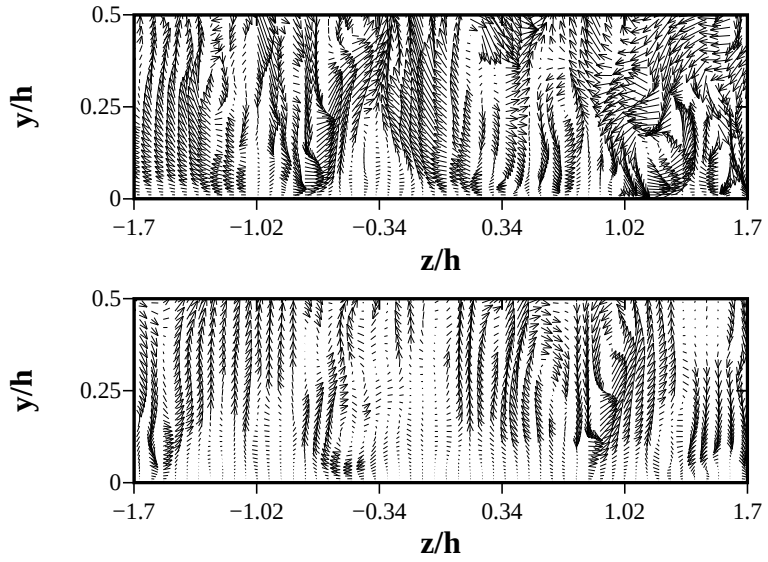

Figure 17: Backward-facing-step: instantaneous field of transverse motion $(w/U_o, v/U_o)$ in the cross-flow plane at $x/h = 7$ (upper plot) and $x/h = 15$ (lower plot)

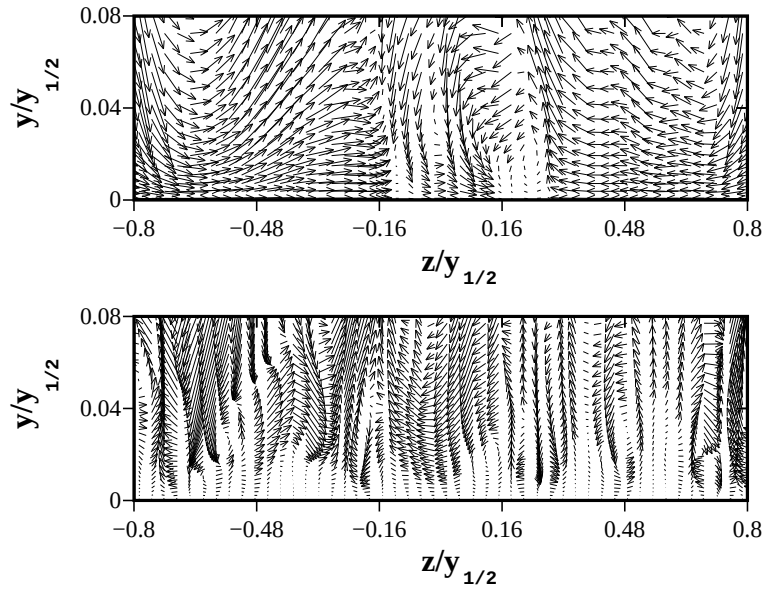

Figure 18: Jet flows: instantaneous field of transverse motion $(w/U_o, v/U_o)$ in the cross-flow plane at $x/b = 20$, zero-wall-shear jet (upper plot), real jet (lower plot)

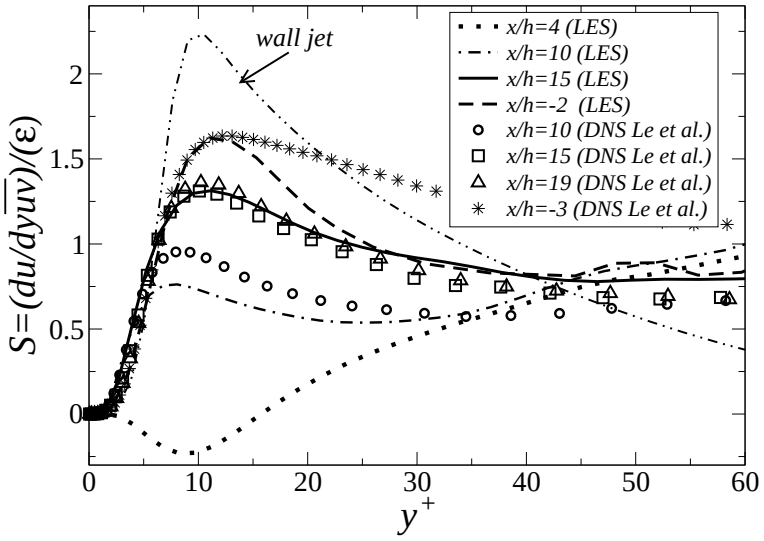

Figure 19: Evolution of the shear-strain parameter, $\tilde{S}$, along the streamwise direction of the back-step flow; comparison with the wall jets

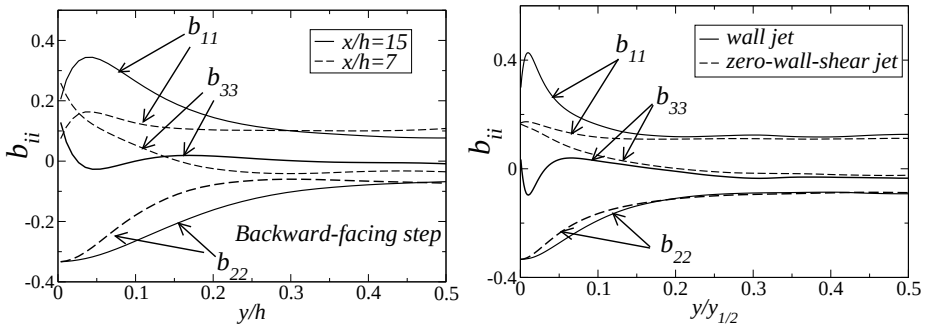

Figure 20: Profiles of the normal-stress anisotropy

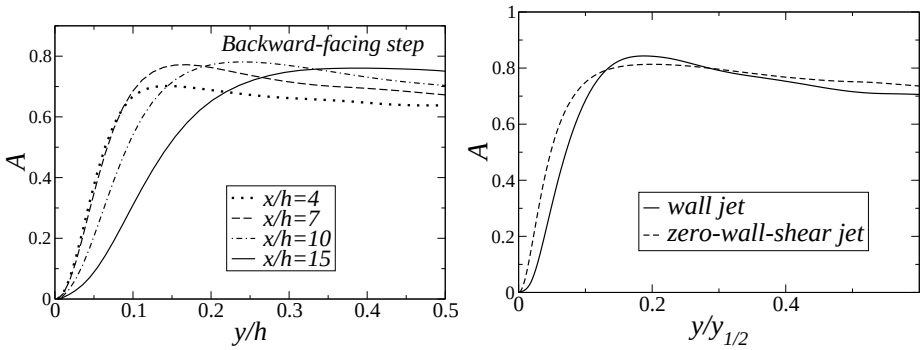

Figure 21: Backward-facing-step flow: profiles of the flatness parameter

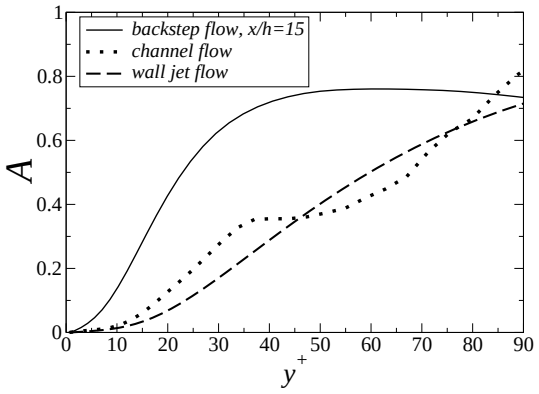

Figure 22: Jet flows: profiles of the flatness parameter

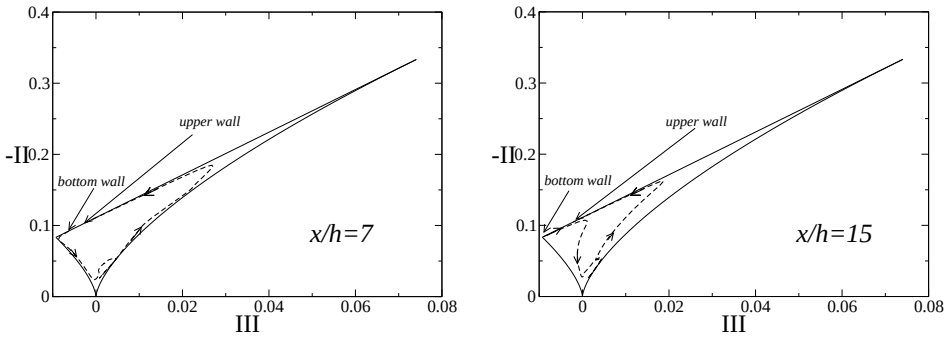

Figure 23: Backward-facing-step flow: anisotropy maps

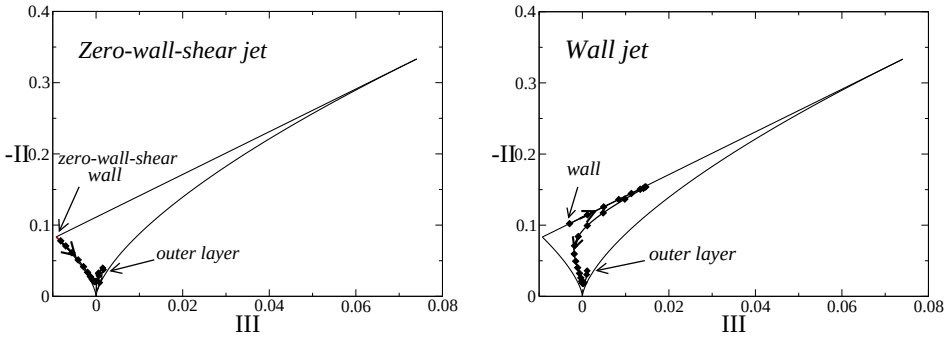

Figure 24: Jet flows: anisotropy maps

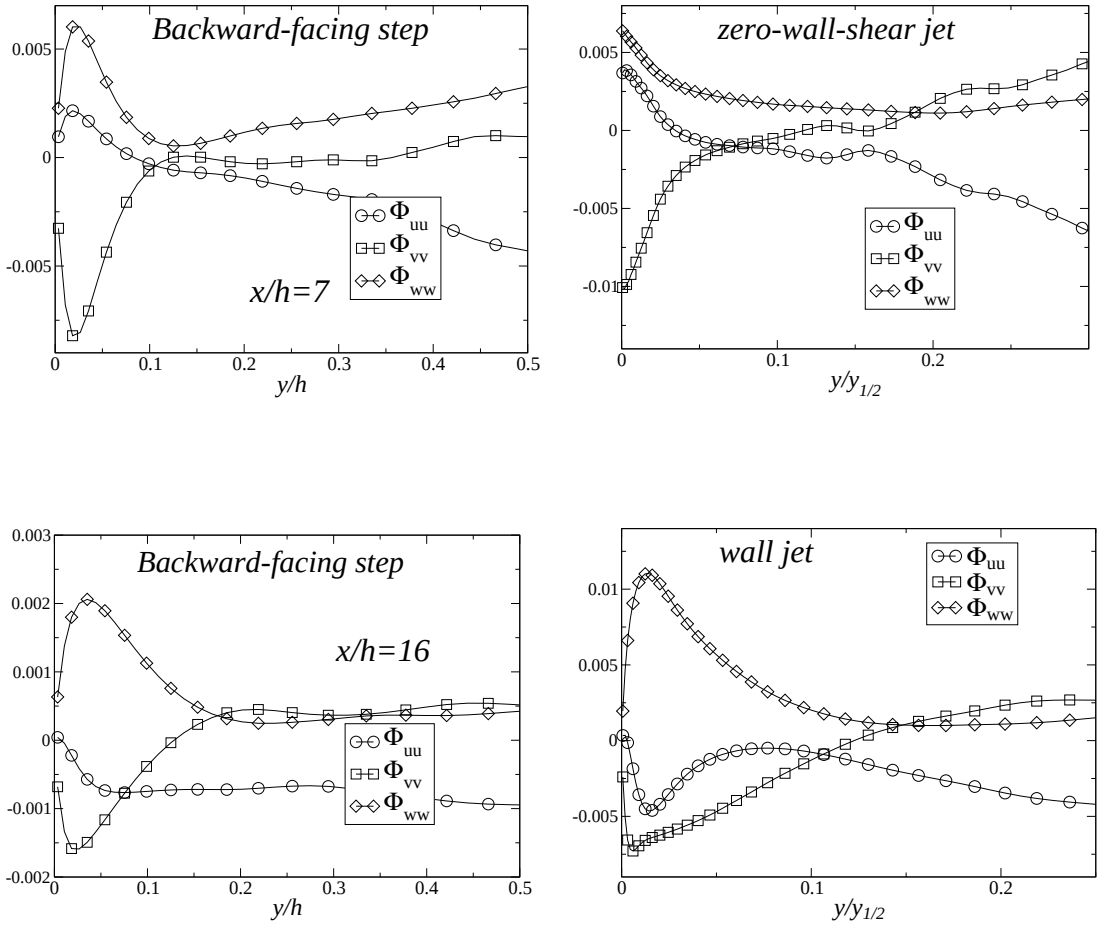

Figure 25: Redistribution of turbulence energy through the pressure-strain term, Φ_{ij}

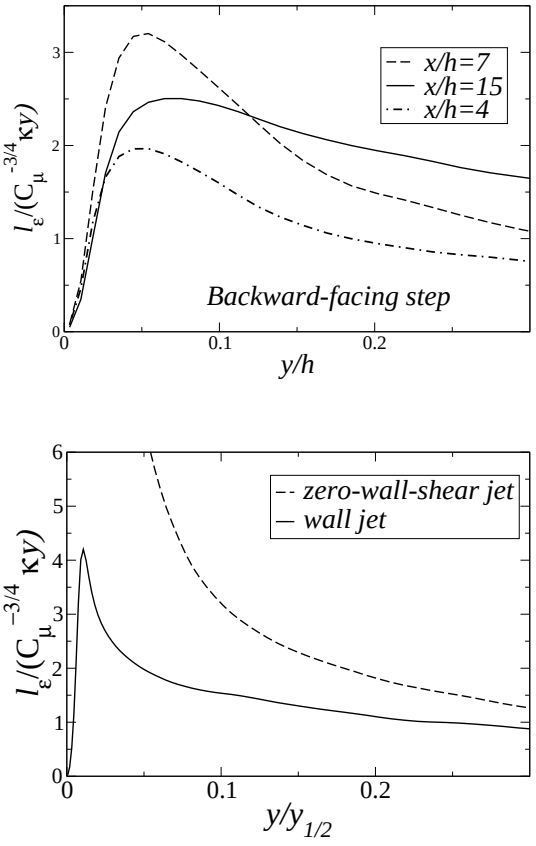

Figure 26: Integral length scale, $l_\varepsilon = k^{3/2}/\varepsilon$, normalised by the equilibrium value

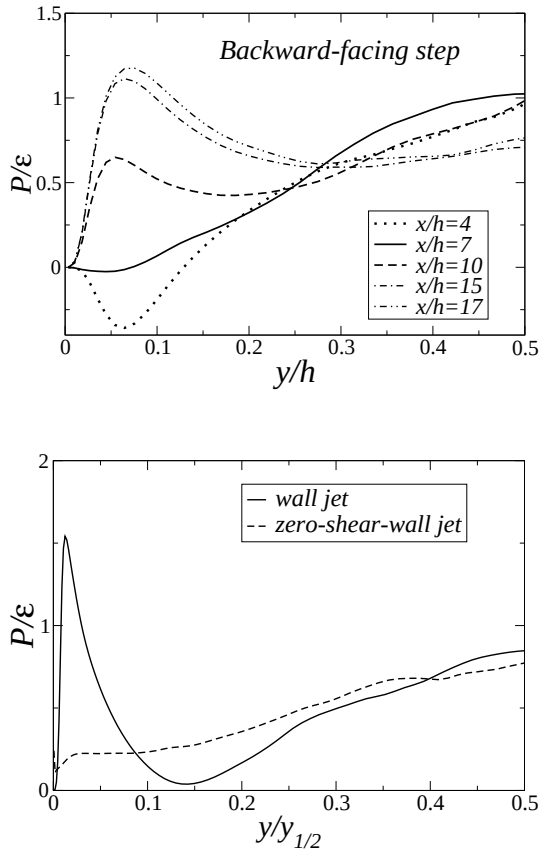

Figure 27: Ratio of turbulence-energy production P to its dissipation ε of turbulence energy.